PAPER

Check for updates

Experimental and theoretical investigations of divinylbenzene-based polymer as an efficient adsorbent for brilliant green dye removal†

Marwa Magdy,[a] Mohamed M. Aboelnga,[ab] Aya Deyab,[a] Aliaa Semida,[a] Rawan Rizk,[a] Nada Elseady,[a] Mona Abo Hashesh[a] and Elsayed Elbayoumy ✦[a]

Water contamination caused by synthetic dyes is a growing environmental concern, necessitating the development of effective and sustainable remediation technologies. In this study, poly(divinylbenzene) (poly(DVB)) was synthesized *via* suspension polymerization and evaluated as a novel adsorbent for the removal of Brilliant Green (BG) dye from aqueous solutions. Characterization techniques including Fourier-transform infrared spectroscopy (FTIR), thermogravimetric analysis (TGA), scanning electron microscopy (SEM), X-ray diffraction (XRD), and Brunauer–Emmett–Teller (BET) surface area analysis confirmed the polymer's porous morphology, thermal stability, and adsorption potential. Batch adsorption experiments were conducted to assess the influence of key operational parameters, and the results showed that the highest removal efficiency of 97.4% was achieved under optimal conditions of pH 7, temperature 298 K, contact time of 120 minutes, initial dye concentration of 7.5 mg L^{-1} and adsorbent dose of 0.05 g 10 ml^{-1}. The adsorption kinetics followed the pseudo-second-order model, suggesting that chemisorption dominates the process, while isotherm modeling indicated that monolayer adsorption occurred on a homogeneous surface, as described by the Langmuir model. Thermodynamic analysis revealed that the adsorption process was endothermic and spontaneous, confirming enhanced dye–polymer interactions at elevated temperatures. DFT calculations were then applied to provide novel atomistic details that should help in better understanding of the chemical interaction that takes place between the dye and the adsorbent. Furthermore, regeneration studies demonstrated that poly(DVB) was sustainable and can be reused for up to four cycles, supporting its feasibility for real-world wastewater treatment applications. Comparisons with previously reported adsorbents highlighted the superior performance of poly(DVB), making it a promising, adsorbent for dye removal from contaminated water.

1. Introduction

Environmental pollution caused by water and wastewater contamination is one of the most pressing global challenges. The aquatic environment is continuously polluted by human activities, particularly through the discharge of industrial effluents containing oil, heavy metals, and synthetic dyes.[1–3] Synthetic dyes are extensively used across various industries, including textiles, leather, plastics, cosmetics, food processing, paper, paints, pulp, carpets, hair coloring, and printing inks.[4–8]

[a]*Chemistry Department, Faculty of Science, Damietta University, New Damietta 34517, Egypt. E-mail: marwasleem@du.edu.eg; Mohamed.aboelnga@du.edu.eg; ayamarz44@gmail.com; aliaahesham152@gmail.com; rewangamal106@gmail.com; dodomhmd58@gmail.com; monamohamedabohashesh@gmail.com; sayedelbayoumy@du.edu.eg*

[b]*King Salman International University, Faculty of Basic Sciences, Ras Sudr, South Sinai, 46612, Egypt*

† Electronic supplementary information (ESI) available. See DOI: https://doi.org/10.1039/d5ra02950c

As a result, approximately 10–15% of the annual production of over 100 000 synthetic dyes amounting to nearly 800 000 tons is released into water bodies, contaminating freshwater resources and severely impacting aquatic ecosystems.[9]

These pollutants frequently exceed the permissible limits set by the World Health Organization (WHO), raising significant environmental and health concerns due to their high toxicity and low degradability.[10,11] Moreover, dye pollutants can obstruct sunlight penetration in water bodies, disrupting photosynthesis and harming aquatic flora and fauna.[12] Many dyes, including BG, exhibit carcinogenic and mutagenic properties, posing serious health risks such as nervous system disorders, liver and kidney failure, eye and skin irritation, respiratory problems, and even cancer.[13–18] However, BG is currently being utilized in different industrial and medical applications, such as coloring paper, silk, wool, rubber and leather as well as in veterinary medicine, and pharmaceutical industry. The presence of such toxic compounds degrades water quality, rendering it unsuitable for drinking, agriculture, and other essential uses while

threatening both human health and ecological sustainability. Specific maximum permissible concentration limits may vary by region, studies and environmental guidelines suggest that the concentration of dyes like BG in discharged wastewater should not exceed 0.01–0.1 mg L^{-1}, depending on local regulations, to prevent harmful ecological effects. Therefore, immediate action is required to develop effective wastewater treatment strategies and explore safer alternatives to mitigate dye pollution.

Various techniques have been employed to remove toxic dyes from wastewater, including oxidation, electrolysis, membrane filtration, adsorption, microbiological and enzymatic treatments, flocculation-precipitation, electrochemical processes, and photocatalytic degradation.[19–21] Among these, adsorption is widely recognized as one of the most effective methods due to its cost-efficiency, simplicity, high removal capacity, and suitability for large-scale applications.[22] The success of adsorption technology depends on selecting an adsorbent with a strong affinity for the target dye, high adsorption capacity, low cost, and high efficiency. Numerous adsorbents, including polymers, nanoparticles, activated carbon, zeolites, and metal–organic frameworks, have been explored for dye removal.[23]

For example, hydroxyapatite (HAp) synthesized from cost-effective precursors within a chitosan (CS) matrix has been used as an adsorbent to remove BG dye from contaminated water solutions.[24] Similarly, activated carbon derived from waste banana peels has demonstrated effectiveness in removing cationic BG dye from aqueous media.[25] Molecularly imprinted polymers (MIPs) have also been employed for the adsorption of BG dye from textile industry effluents and river water.[26] Among polymeric materials, poly(divinylbenzene) (poly(DVB)) has emerged as a promising adsorbent due to its unique structural properties, including a high surface area and large pore radius,

which enhance its ability to adsorb contaminants from aqueous solutions.[27,28] Also, it has gained to be excellent adsorbent due to its easy fabrication process, low cost, recyclability, strong adsorption capacity, environmental stability, and suitability for large-scale use. The presence of aromatic rings in poly(DVB) is particularly advantageous, as it facilitates effective coordination with dye molecules which improves the efficiency of dye removal, making poly(DVB) an effective material for applications in water purification. Also, due to its hydrophobic and rigid aromatic structure, it is generally considered non-biodegradable in typical environmental settings which make it suitable for different industrial applications. Additionally, its exceptional thermal stability allows for large-scale applications under diverse operating conditions.[29]

In this study, poly(DVB) was synthesized using the suspension polymerization technique and subsequently employed as an adsorbent for the extraction of BG dye from aqueous solutions. The synthesized polymer was characterized using FTIR, TGA, SEM, XRD, and BET techniques to evaluate its structural, thermal, and morphological properties. The effects of key operational parameters, including contact time, adsorbent dosage, initial dye concentration, temperature, and pH, on the adsorption efficiency were systematically investigated (Fig. 1). Additionally, adsorption kinetics, isotherm models, and thermodynamic parameters were analyzed to understand the underlying mechanisms governing the adsorption process. To obtain deeper structural insights into the complex, we have computationally modelled the interaction that occurs between the BG dye and the adsorbent. The findings of this study present a practical and efficient approach for removing BG dye from wastewater using poly(DVB), highlighting its potential for large-scale wastewater treatment applications.
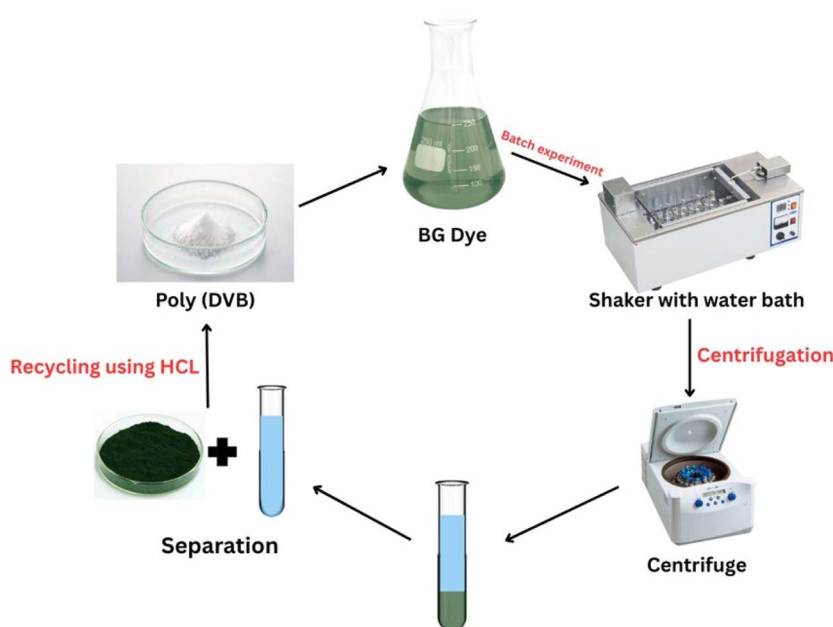

Fig. 1 Batch experiment for the removal of hazardous BG dye using poly(DVB).

2. Material and methods

2.1. Materials

Divinylbenzene (DVB) was purchased from TCI (Tokyo, Japan). α,α′-Azobisisobutyronitrile (AIBN, purity >98%) was purchased from Wako Chemical (Osaka, Japan). Polyvinyl alcohol (PVA) was obtained from Sigma-Aldrich, and toluene (purity >99.5%) was purchased from Merck (Darmstadt, Germany). Ethanol, acetone, sodium hydroxide, hydrochloric acid, and potassium nitrate were obtained from Fisher Scientific. Brilliant Green dye (BG) was obtained from Aldrich Chemicals. AIBN was recrystallized from ethanol, and acetonitrile was distilled before use. All other chemicals were used as received without further purification.

2.2. Synthesis of poly(DVB)

Poly(DVB) was synthesized using suspension polymerization techniques, as previously described, with slight modifications.[30] The synthesis scheme of divinylbenzene Polymer was shown in Fig. 2. In our modified approach, the organic phase solution consisted of DVB monomer (74.04 mmol, 2 ml), AIBN initiator (39.97 mg), and toluene (2 ml) as a diluent. This differs from the original method, which used a mixture of toluene and heptane. The exclusive use of toluene in our method simplifies the system and results in a more uniform pore structure. The organic phase was added to 16 ml of an aqueous phase (0.5% PVA) and stirred for 10 minutes at 10 °C. The reaction mixture was then heated to 60 °C and maintained for 24 hours. After completion, the reaction was quenched to room temperature, and the resulting white precipitate of poly(DVB) was separated by filtration. It was then washed several times with ethanol and acetone to remove any unreacted monomer or initiator. Finally, the obtained poly(DVB) was dried under vacuum and stored for further use.

2.3. Characterization techniques

Fourier transform infrared (FTIR) spectroscopy was conducted on a JASCO FT/IR-6100 spectrometer using KBr pellet samples, covering the spectral range of 4000–400 cm^{-1} to identify functional groups present in the polymer. Thermal gravimetric analysis (TGA) was performed using a Rigaku Thermo plus TG8120 instrument under a nitrogen atmosphere (flow rate: 20 ml min^{-1}) at a heating rate of 10 K min^{-1}, using an alumina ceramic sample from room temperature up to 800 °C, to evaluate the thermal stability of the polymer. Wide-angle X-ray

Fig. 2 Schematic represented the synthesis of poly(DVB).

diffraction (XRD) analysis was performed using a Siemens D-500 diffractometer (λ = 1.54 Å, Cu Kα) to investigate the crystalline structure and crystalline size of the copolymer. Nitrogen adsorption/desorption measurements were carried out with a Quantachrome instrument (USA) to determine the surface area and pore volume of the copolymer, based on the Brunauer–Emmett–Teller (BET) method. To investigate the micromorphological and microtextural features of copolymer the scanning electron microscopy (SEM) was employed with JEM-2100F microscopy at an accelerating voltage of 200 kV.

2.4. Batch adsorption experiments

To investigate adsorption parameters, including isotherm, kinetics, and thermodynamics, batch adsorption experiments were conducted in 250 ml bottles at room temperature. A fixed amount of the adsorbent under investigation was added to 100 ml of BG solution, which was then adjusted to the desired pH. After adding the known amount of adsorbent, the bottles were shaken in a thermostatic shaker at 200 rpm for variable duration. At the end of the equilibrium period, the sample containing both dye and adsorbent was centrifuged for 10 minutes, and the remaining dye concentration was measured using a UV-vis spectrophotometer at wavelength 625 nm, corresponding to the equilibrium concentration of BG (C_e). During the experiments, the effects of various adsorption parameters, including adsorption time (5 to 170 minutes), pH (3 to 9), initial dye concentration (2 to 14.3 ppm), adsorbent dose (0.02 to 0.18 g), and temperature (303 to 333 K), were systematically examined to determine the optimal conditions for the adsorption process. The adsorption capacity (q_t) of BG onto poly(DVB) and dye removal percentage (% R) were calculated using the following equation:

$$q_t = \frac{C_o - C_t}{W} \times V \tag{1}$$

$$\% R = \frac{C_o - C_t}{C_o} \times 100 \tag{2}$$

where C_0 is the initial dye concentration (mg L^{-1}), C_t is the dye concentration at time t (mg L^{-1}), W is the adsorbent mass (g), and V is the volume of the BG dye solution (L). To ensure reproducibility, each batch adsorption experiment was conducted in triplicate. The reported results represent the mean values, with error bars (standard deviations) included where applicable. The standard deviation across replicates was consistently below 5%, confirming the robustness and reliability of the experimental findings.

2.5. Computational investigation

To deepen our understanding of the adsorption mechanism, we have expanded our investigation into computationally study the binding of our dye on the surface of the polymer. A representative moiety for the polymer was loaded with our dye and explored using DFT calculations implementing Gaussian09 software.[31] In particular, B3LYP functional[32–34] in combination with 6-31G basis set has been employed to perform complete
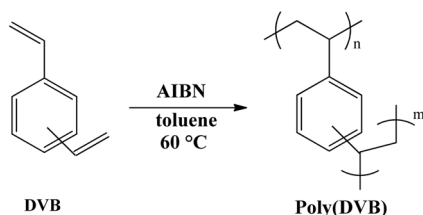
geometry optimization for the complex. In fact, this combination of methods have been successfully used by our group to treat different chemical systems.[35,36] The highest occupied molecular orbital (HOMO) and the lowest occupied molecular orbital (LUMO) have been also displayed utilizing Gaussview software to further broaden our knowledge for the types of chemical interactions that take place during the adsorption.

3. Results and discussion

3.1. Adsorbent characterization

3.1.1. FTIR analysis. The FTIR spectrum of poly(DVB), presented in Fig. 3A, provides insight into the polymer's functional groups. The presence of characteristic peaks in the range of $3021.97–2916.43$ cm^{-1} corresponds to the stretching vibrations of aliphatic C–H bonds, confirming the incorporation of aliphatic structures within the polymer network.[37] Additionally, the absorption bands observed between 1691.26 cm^{-1} and 1442.9 cm^{-1} are attributed to C=C stretching, indicating the presence of aromatic rings.[38] Furthermore, the sharp absorption band at 714 cm^{-1} is associated with out-of-plane ring deformation, which is a typical feature of benzene-derived compounds, further supporting the polymer's aromatic character.[39] The distinct peak at 1594.82 cm^{-1} is characteristic of aromatic ring vibrations, reinforcing the presence of benzene moieties in the polymer backbone. Moreover, the absorption bands appearing at 900 cm^{-1} and 989 cm^{-1} correspond to vinyl group vibrations, which indicate residual unsaturation from the polymerization process.[38]

The FTIR spectrum of poly(DVB) after BG dye adsorption is shown in Fig. S1 in ESI.† Compared to the spectrum of the pristine polymer, the major characteristic bands of poly(DVB) remain intact, including the aromatic C=C stretching (~ 1590 cm^{-1} and 1440 cm^{-1}) and C–H bending (~ 714 cm^{-1}), confirming the structural stability of the polymer matrix during the adsorption process. However, several notable changes indicate successful interaction with the BG dye. A slight shift and broadening is observed in the C=C aromatic region (~ 1595 cm^{-1}), suggesting π–π interactions between the aromatic rings of the dye and the polymer. The band at ~ 900–989 cm^{-1}, attributed to vinyl groups, appears less intense, which could be due to coverage or interaction of dye molecules with residual unsaturated sites. These spectral changes provide strong evidence of chemical interactions particularly π–π stacking between BG dye and the poly(DVB) framework, supporting the proposed chemisorption mechanism.

3.1.2. Thermal gravimetric analysis (TGA). The thermal stability of poly(DVB) was evaluated using thermogravimetric analysis (TGA) and derivative thermogravimetric analysis (DTG), as illustrated in Fig. 3B. The TGA curve demonstrates a two-step degradation process. The first stage, occurring between 46 °C and 156 °C, exhibits a slight weight loss, which is likely due to the evaporation of residual moisture and organic solvents trapped within the polymer matrix.[40] Beyond 240 °C, a significant increase in weight loss occurs, peaking at 425 °C, as indicated by the DTG curve. This stage, which corresponds to a weight loss of 34.91%, represents the major thermal degradation of the polymer, where the polymer backbone undergoes decomposition.[41] The high degradation temperature suggests that poly(DVB) possesses strong thermal stability, likely due to its crosslinked aromatic structure, which enhances resistance to thermal breakdown. To further understand the thermal
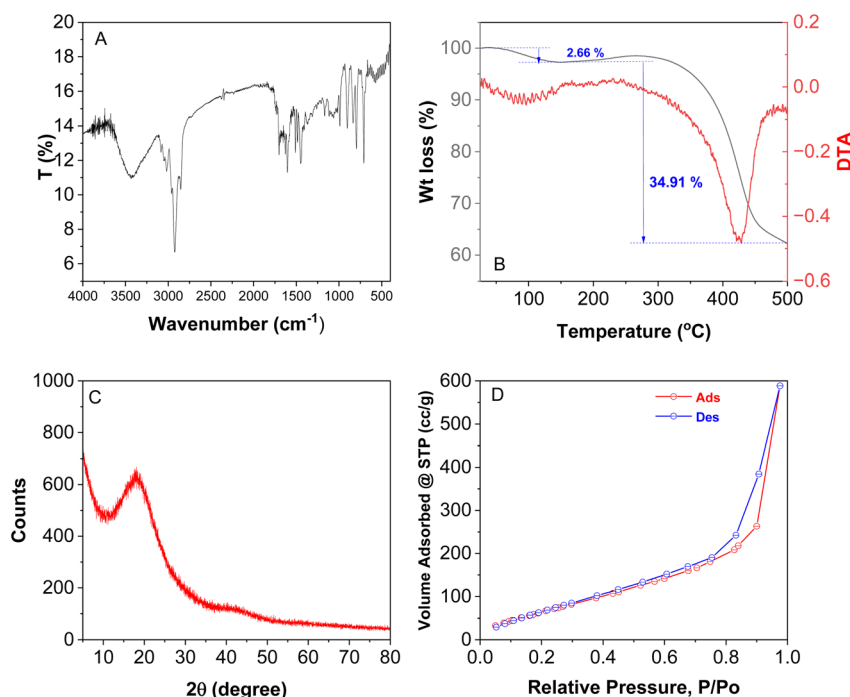

Fig. 3 (A) FTIR spectra; (B) TGA analysis; (C) XRD analysis; (D) BET analysis of poly(DVB).

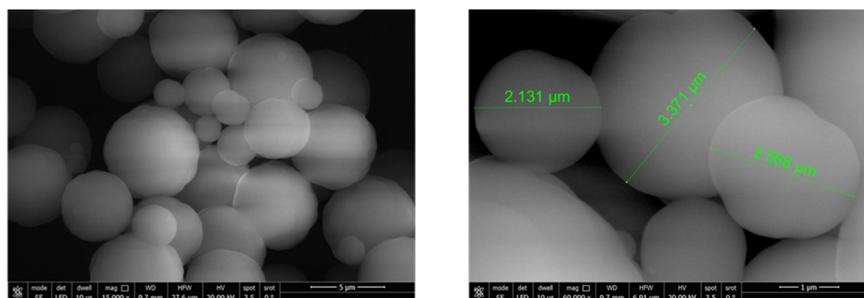**Table 1** Thermal activation energy and thermodynamic parameters of poly(DVB)

E^* (kJ mol^{-1})	A' (S^{-1})	ΔS^* (J mol^{-1} K^{-1})	ΔH^* (kJ mol^{-1})	ΔG^* (kJ mol^{-1})
78.84166	1093.711	−189.753	75.2925	156.296

degradation kinetics, the Coats–Redfern method was applied to determine the activation energy (E^*) and thermodynamic parameters (ΔH^*, ΔS^*, and ΔG^*) of the main degradation stage (240–500 °C). As shown in Table 1, the calculated activation energy (E^*) of 78.84 kJ mol^{-1} suggests a relatively high energy barrier for decomposition, reinforcing the polymer's thermal stability. The positive enthalpy change ($\Delta H^* = 75.29$ kJ mol^{-1}) confirms that the degradation process is endothermic, requiring energy input to proceed 363 636.[42,43] Additionally, the negative entropy change ($\Delta S^* = -189.75$ J mol^{-1} K^{-1}) suggests that the degradation reaction leads to a more ordered transition state, potentially due to the formation of intermediate structures before complete breakdown. Furthermore, the high Gibbs free energy ($\Delta G^* = 156.30$ kJ mol^{-1}) indicates that the degradation process is non-spontaneous, requiring external energy to initiate polymer decomposition. Overall, the TGA results confirm that poly(DVB) exhibits strong thermal stability up to 240 °C, with a major degradation onset above 400 °C, making it a promising material for applications that demand thermal resistance and structural durability.

3.1.3. XRD analysis. The crystalline structure of poly(DVB) was investigated using X-ray diffraction (XRD), and the corresponding diffraction pattern is shown in Fig. 3C. The XRD analysis reveals a broad peak centered at $2\theta = 18.18°$, indicating that poly(DVB) exhibits a predominantly amorphous structure 373 737. The absence of sharp, well-defined diffraction peaks suggests that the polymer lacks long-range molecular order, which is characteristic of highly crosslinked and disordered polymer networks. The amorphous nature of poly(DVB) can be attributed to the presence of irregularly arranged aromatic rings and crosslinked polymer chains, which hinder the formation of crystalline domains. This structural characteristic significantly influences the material's mechanical, optical, and sorption properties, making it suitable for applications requiring high flexibility, optical transparency, and enhanced adsorption capabilities.[44]

3.1.4. Brunauer–Emmett–Teller analysis (BET). The surface area and porosity of poly(DVB) were evaluated using BET analysis, based on nitrogen adsorption/desorption isotherms at 77 K. The corresponding isotherm is shown in Fig. 3D. The results indicate that poly(DVB) exhibits a high specific surface area of 249.47 m^2 g^{-1}, suggesting a well-developed porous structure. Additionally, the Barrett–Joyner–Halenda (BJH) method was used to determine the pore volume and pore radius of the polymer. The total pore volume was measured at 0.877 cm^3 g^{-1}, while the pore radius was calculated as 1.633 nm. According to the International Union of Pure and Applied Chemistry (IUPAC) classification, materials with pore diameters below 2 nm are categorized as microporous.[45] Based on these values, poly(DVB) falls within the microporous range, making it suitable for applications requiring high surface area and fine porosity, such as adsorption, separation, and catalysis. Furthermore, the microporous nature of poly(DVB) suggests strong potential for gas and liquid adsorption, positioning it as a promising adsorbent material. Furthermore, its high surface area enhances adsorption efficiency and reactivity. To further investigate the structural changes following dye adsorption, BET surface area analysis was also conducted on poly(DVB) after BG dye adsorption (Fig. S2 in ESI†). The results showed a significant decrease in surface area from 249.47 m^2 g^{-1} to 93.54 m^2 g^{-1}, indicating that a substantial portion of the accessible surface became occupied or blocked by adsorbed dye molecules. Similarly, the total pore volume decreased from 0.877 cm^3 g^{-1} to 0.106 cm^3 g^{-1}, and the average pore radius slightly reduced from 1.633 nm to 1.551 nm. These reductions provide strong evidence that BG dye molecules were successfully adsorbed into the porous structure of the polymer, occupying both external and internal adsorption sites. This result supports the adsorption mechanism inferred from isotherm and kinetic modeling, where dye–polymer interaction is likely dominated by surface binding and pore filling processes.

3.1.5. SEM analysis. The morphology and particle size distribution of poly(DVB) were analyzed using scanning

Fig. 4 SEM images of poly(DVB).

electron microscopy (SEM), as shown in Fig. 4. The SEM images reveal that poly(DVB) exhibits an irregular spherical morphology, with particles varying in size. The measured average particle size is approximately 2.69 μm, indicating a relatively uniform distribution with slight variations. The spherical shape suggests that the polymerization process facilitated the formation of well-defined microspheres. However, the observed irregularities in shape and size may result from variations in polymerization kinetics, crosslinking density, or reaction conditions, such as monomer concentration, solvent system, and initiator type. Furthermore, the high-magnification SEM image provides a clearer view of the surface texture and particle connectivity, which play a crucial role in determining the adsorption properties, surface reactivity, and packing density of the material. The relatively uniform particle size distribution enhances the potential applications of poly(DVB) in adsorption, catalysis, and separation processes, where controlled morphology and high surface area are essential. Additionally, the morphology of poly(DVB) after adsorption of BG dye was examined by SEM analysis and the results are presented in Fig. S3 in ESI.† The overall particle morphology remained similar to that of free poly(DVB), with no significant visual changes in surface texture or aggregation observed at this resolution. This suggests that BG dye adsorption occurs primarily through surface-level or molecular–scale interactions that may not produce detectable morphological changes under SEM. These findings are consistent with the adsorption being a chemisorption-dominated process, as supported by FTIR and BET.

3.2. Adsorption batch experiment

3.2.1. Point of zero charge (PZC).
The point of zero charge (PZC) represents the pH at which the net surface charge of an adsorbent is neutral. This parameter is crucial in understanding the adsorption behavior of poly(DVB), as it determines the surface charge properties in different pH environments. The PZC of poly(DVB) was determined experimentally using 0.1 M KNO$_3$ solutions with varying initial pH values [3–9], adjusted using 0.1 M HCl and 0.1 M NaOH. After equilibration with 0.05 g of poly(DVB) for 48 hours at room temperature, the final pH values were recorded, and the PZC was determined. As shown in Fig. 5A, the PZC of poly(DVB) was found to be 8.2. This result indicates that at pH values below 8.2, the surface of poly(DVB) carries a positive charge, favoring the adsorption of negatively charged species (*e.g.*, anionic dyes or pollutants). Conversely, at pH values above 8.2, the surface charge becomes negative, enhancing the interaction with positively charged species (*e.g.*, cationic dyes or heavy metal ions).[46] Understanding the PZC of poly(DVB) is essential for optimizing its adsorption efficiency, as the electrostatic interactions between the adsorbent and target contaminants strongly depend on the solution pH. This makes poly(DVB) a versatile material for various adsorption applications where charge-dependent interactions play a significant role.

3.2.2. Effect of pH.
The effect of pH on the adsorption of BG dye onto poly(DVB) is illustrated in Fig. 5B. The results indicate that the removal efficiency of BG dye significantly increases as the pH rises from 3 to 7, reaching a maximum adsorption efficiency of 82.65% at pH 7. Beyond this optimal pH, the removal percentage declines as the pH increases above 7. This trend can be attributed to the cationic nature of BG dye, which remains positively charged in solution. At lower pH values, the concentration of H$^+$ ions is high, leading to increased competition between H$^+$ and BG dye molecules for the active adsorption sites on the surface of poly(DVB). This competition reduces the adsorption efficiency at acidic conditions. As the pH increases, the surface of poly(DVB) becomes more negatively charged, enhancing the electrostatic attraction between the adsorbent and the cationic BG dye molecules.[47] This explains the observed increase in removal efficiency up to pH 7. However, at pH values higher than 7, the adsorption efficiency declines. This reduction may be due to the decreased positive charge on the dye molecules and possible repulsion effects, which weaken the electrostatic interactions between the adsorbent and the dye.[48] Additionally, changes in the chemical structure of the dye at higher pH levels could contribute to lower adsorption rates. Overall, the results confirm that electrostatic interactions play a crucial role in BG dye adsorption onto poly(DVB). Since pH 7 yielded the highest removal efficiency, it was selected as the optimal pH for subsequent adsorption experiments.

3.2.3. Effect of contact time.
The influence of contact time on the adsorption of BG dye onto poly(DVB) is presented in Fig. 5C. The results indicate that the removal efficiency (% R) and adsorption capacity (q_e) of BG dye increase steadily with contact time until equilibrium is reached. Throughout the adsorption process, the removal percentage of BG dye shows a continuous and consistent increase without significant fluctuations. This behavior suggests that the adsorption sites on poly(DVB) remain accessible for dye molecules over time, allowing for a gradual and sustained adsorption. The steady increase in adsorption efficiency indicates that diffusion and interaction between dye molecules and the adsorbent surface occur smoothly without noticeable saturation effects within the studied time frame.[49,50] The results suggest that prolonging the contact time enhances adsorption without a distinct plateau phase, implying that the adsorption equilibrium is reached progressively. This highlights the strong affinity of poly(DVB) toward BG dye, making it a promising adsorbent for effective dye removal.

3.2.4. Effect of dye concentration.
The initial dye concentration is a key parameter influencing the adsorption process, as it determines the driving force for mass transfer between the solution and the adsorbent. Fig. 5D illustrates the effect of initial dye concentration on the adsorption efficiency of BG dye using poly(DVB). The results show that as the initial BG dye concentration increases from 2.5 to 14.3 ppm, the dye removal percentage (% R) decreases from 63.9% to 32.5%. This decline in removal efficiency can be attributed to the saturation of available adsorption sites on the polymer surface at higher dye concentrations. As the number of dye molecules in solution increases, the fixed number of active adsorption sites becomes a limiting factor, resulting in excess dye molecules remaining unadsorbed in solution. Despite the decrease in removal
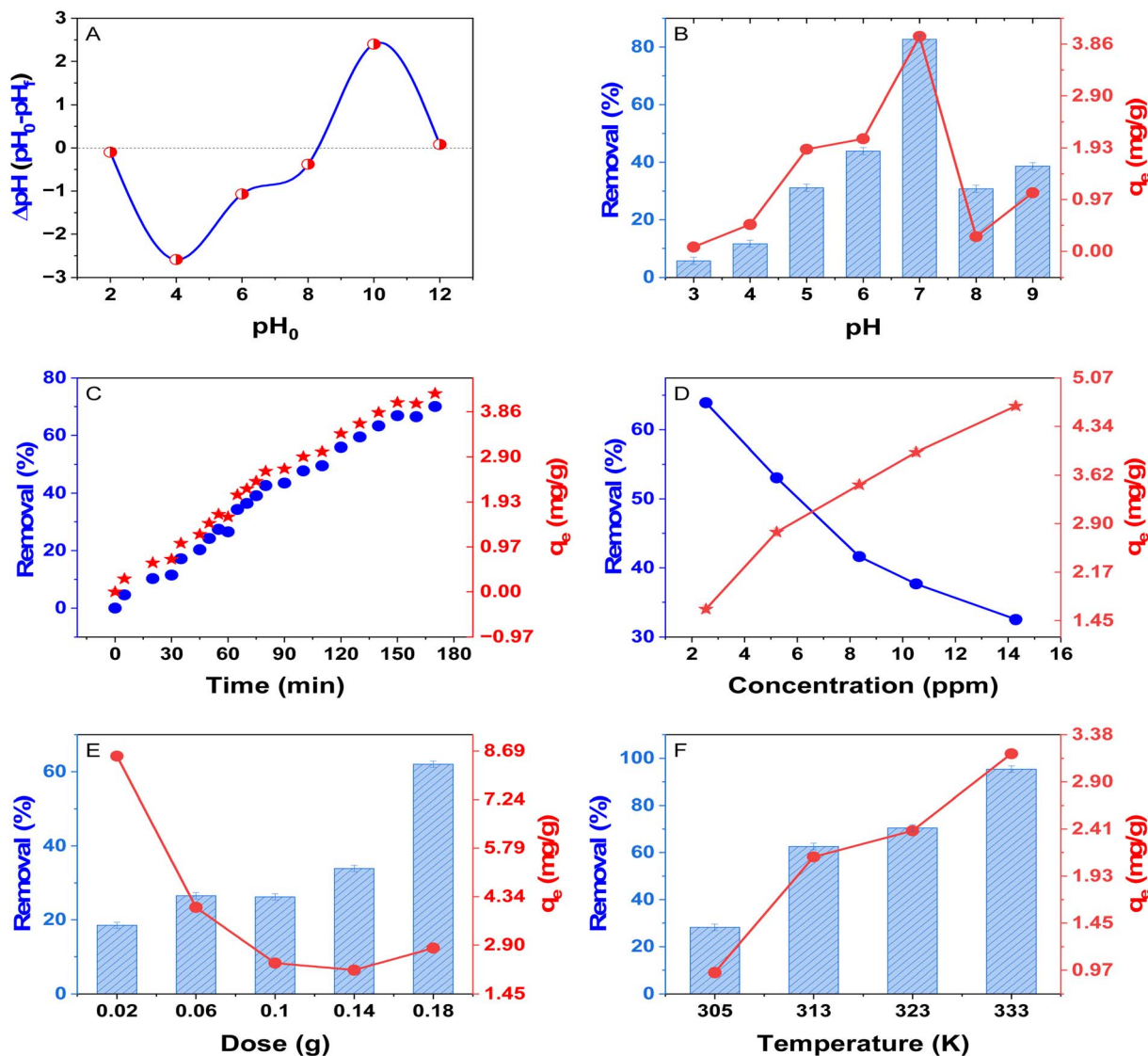
Fig. 5 (A) Point of zero charge (PZC); (B) effect of PH; (C) effect of contact time; (D) effect of dye concentration; (E) effect of adsorbent dose; (F) effect of adsorption temperature. Adsorption conditions: (B) pH from 3 to 9, time 60 minutes, 7.5 ppm initial dye concentration, dose 0.1 g/ 25 ml, 298 K; (C) time (0–170 minutes), 7.5 ppm initial dye concentration, dose 0.1 g/100 ml, pH = 7, 298 K; (D) initial dye concentration (2.5–20 ppm), dose 0.1 g/25 ml, pH = 7, 298 K and time 120 minutes; (E) dose (0.02–0.18 g)/100 ml, 7.5 ppm initial dye concentration, pH = 7, 298 K and time 60 minutes; (F) temperature (305–333 k), pH = 7, initial dye concentration = 7.5 ppm, dose = 0.02 g/10 ml and time 60 minutes.

efficiency, the adsorption capacity (q_e) of poly(DVB) increases from 1.59 to 4.63 mg g^{-1} with increasing initial dye concentration. This trend suggests that higher concentrations provide a stronger concentration gradient, enhancing the interaction between dye molecules and available binding sites on the adsorbent. At higher initial concentrations, the probability of dye molecules colliding with and adhering to the adsorbent increases, thereby raising the amount of dye adsorbed per gram of polymer. This phenomenon aligns with previous studies that demonstrate the dependence of adsorption capacity on initial solute concentration, as higher concentrations typically drive a more efficient uptake until saturation is reached.[51,52]

3.2.5. Effect of adsorbent dose. The influence of poly(DVB) dosage on BG dye adsorption was investigated by varying the adsorbent mass from 0.02 to 0.18 g while keeping all other parameters constant. Fig. 5E illustrates the relationship between adsorbent dose and both the removal efficiency (% R) and adsorption capacity (q_e). The results indicate that as the adsorbent dose increases from 0.02 to 0.18 g, the removal percentage of BG dye rises significantly from 18% to 64%. This enhancement in removal efficiency can be attributed to the increased availability of active adsorption sites and the greater surface area provided by higher amounts of poly(DVB), allowing more dye molecules to interact and be captured.[53] However, despite the improvement in removal efficiency, the adsorption capacity (q_e) per gram of adsorbent decreases from 8.44 to 2.45 mg g^{-1} with increasing poly(DVB) dosage. This inverse relationship occurs due to a lower adsorbate-to-adsorbent ratio at higher dosages, where excess adsorption sites remain unoccupied due to the limited dye concentration in solution.[52] Based

on these findings, selecting an optimal adsorbent dose depends on the adsorption objective. A dose of 0.02 g is the most effective for maximizing adsorption capacity, making it suitable for applications where a high dye uptake per gram of adsorbent is required. Conversely, for achieving maximum removal efficiency, a higher dosage of 0.18 g is recommended to ensure greater dye elimination from the solution.

3.2.6. Effect of temperature. The influence of temperature on the adsorption of BG dye onto poly(DVB) was examined over a temperature range of 305 to 333 K while maintaining all other experimental conditions constant. Fig. 5F presents the effect of temperature on both the adsorption capacity (q_e) and removal efficiency (% R). The results demonstrate a significant enhancement in the adsorption process with increasing temperature. Specifically, as the temperature rises from 305 K to 333 K, the adsorption capacity increases from 0.94 to 3.13 mg g^{-1}, while the removal efficiency improves markedly from 28.22% to 95.39%. This increase in adsorption efficiency can be attributed to the higher kinetic energy of dye molecules at elevated temperatures, which enhances their diffusion from the bulk solution to the surface of the adsorbent.[54] Additionally, elevated temperatures improve molecular collisions between BG dye molecules and poly(DVB), increasing the likelihood of effective adsorption interactions.[55] These findings suggest that the adsorption of BG dye onto poly(DVB) is an endothermic process, where higher temperatures facilitate greater dye uptake. The enhanced adsorption efficiency at elevated temperatures indicates the potential applicability of poly(DVB) for high-temperature wastewater treatment applications, where dye removal can be optimized by thermal activation of the adsorption process.

3.3. Adsorption isotherms

Adsorption isotherms are essential tools for understanding the interaction between adsorbate molecules and the adsorbent surface at equilibrium. Various isotherm models, including

Fig. 6 Adsorption isotherm models of BG onto poly(DBV).

Langmuir, Freundlich, Dubinin–Radushkevich (D–R), Temkin, Khan, Hill, and Jovanovic, were used to analyze the adsorption behavior of BG dye onto poly(DVB).[56] Fig. 6 presents the non-linear fitting of these models to the experimental data, while Table 2 summarizes the corresponding isotherm parameters. The Langmuir isotherm assumes monolayer adsorption on a homogeneous surface with no interactions between adsorbed molecules. The high correlation coefficient ($R^2 = 0.97$) for Langmuir suggests that the adsorption of BG dye onto poly(DVB) follows this model, indicating uniform adsorption sites and monolayer adsorption behavior. Additionally, the maximum adsorption capacity (q_m) was found to be 5.649 mg g^{-1}, further supporting the efficiency of poly(DVB) as an adsorbent. In contrast, the Freundlich isotherm, which describes multilayer adsorption on heterogeneous surfaces, exhibited a lower correlation coefficient ($R^2 = 0.822$), indicating that multilayer adsorption is less dominant in this system. This suggests that the adsorption process is more likely to be homogeneous rather than heterogeneous. The Dubinin–Radushkevich (D–R) isotherm, which is used to differentiate between physisorption and chemisorption, yielded an adsorption energy (E_a) of 10.721 kJ mol^{-1}. Since values of E_a between 8 and 16 kJ mol^{-1} indicate chemisorption, it can be inferred that the adsorption of BG dye onto poly(DVB) occurs primarily *via* a chemical interaction mechanism rather than simple physical adsorption.[57] However, the D–R model exhibited a moderate fit ($R^2 = 0.80$), indicating that it may not fully describe the adsorption process. The Temkin isotherm, which assumes that the heat of adsorption decreases linearly with increasing surface coverage, showed a good fit ($R^2 = 0.9856$), suggesting the presence of a uniform distribution of binding energies on the poly(DVB) surface. The Khan isotherm, which accounts for solute adsorption onto solid surfaces, and the Hill model, which describes cooperative binding interactions, both provided high correlation coefficients ($R^2 = 0.9965$ and $R^2 = 0.9908$, respectively). This indicates that these models can also describe the adsorption behavior effectively. The Jovanovic isotherm, which modifies the Langmuir model to account for possible mechanical interactions between adsorbed and desorbed molecules, showed a slightly lower fit ($R^2 = 0.9289$) compared to Langmuir. This suggests that while mechanical interactions may occur, they do not significantly impact the adsorption mechanism. Overall, the adsorption of BG dye onto poly(DVB) is best described by the Langmuir model, confirming that the adsorption occurs *via* a monolayer mechanism on a homogeneous surface. The high adsorption energy determined from the D–R model further supports a chemisorption process.

3.4. Adsorption kinetics of BG dye onto poly(DVB)

Adsorption kinetics studies are crucial for understanding the adsorption mechanism, equilibrium time, and rate-controlling steps at the liquid–solid interface. In this study, the adsorption of BG dye onto poly(DVB) was evaluated using four kinetic models: pseudo-first-order (PFORE), pseudo-second-order (PSORE), Elovich, and intra-particle diffusion (IPDE).[58] The
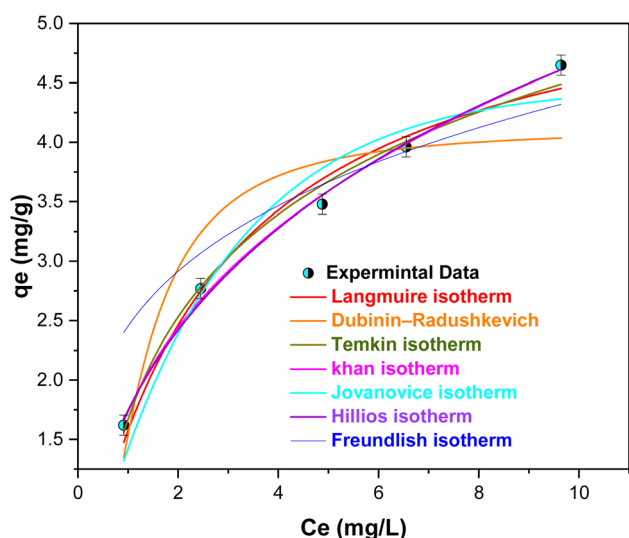
Table 2 Adsorption isotherm parameter of brilliant green dye onto poly(DVB)

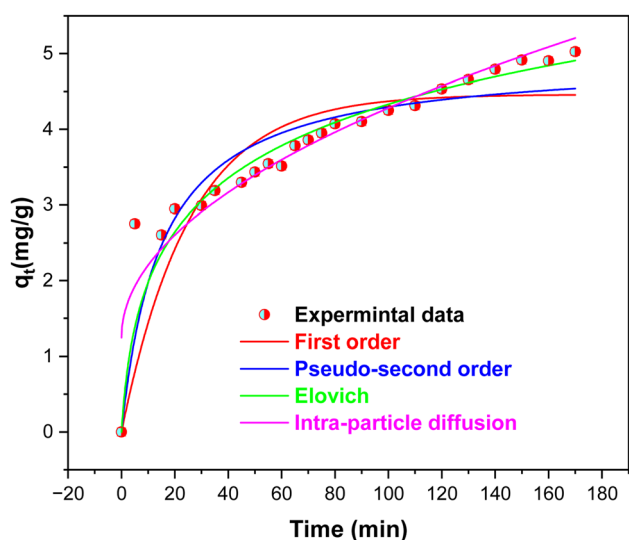| Isotherm	Equation	Parameters	Value
Langmuir	$q_e = (Kq_mC_e)/(1 + KC_e)$	q_m (mg g^{-1})	5.649
		K (L mg^{-1})	0.386
		R-square (COD)	0.979
		R^2	0.972
Freundlich	$q_e = K_F C_e^{1/n}$	K_F (mg g^{-1})	2.451
		$1/n$	0.249
		R-square (COD)	0.822
		R^2	0.822
Dubinin–Radushkevich	$q_e = q_m \exp^{-k\varepsilon^2}$	q_m (mg g^{-1})	4.116
	$\varepsilon = \left[RT \ln \left(1 + \dfrac{1}{C_e} \right) \right]$	k (mol^2 J^{-2})	4.350×10^{-9}
	$E_a = \dfrac{1}{\sqrt{2K}}$	E_a (kJ mol^{-1})	10.721
		R-square (COD)	0.852
		R^2	0.802
Temkin	$q_e = B \ln(k \times C_e)$	B	1.244
		K (L mg^{-1})	3.819
		R-square (COD)	0.989
		R^2	0.985
Khan	$q_e = q_m K C_e /(1 + KC_e)^n$	q_m (mg g^{-1})	1.612
		K	2.405
		n	0.657
		R-square (COD)	0.996
		R^2	0.993
Jovanovic	$q_e = q_m(1 - \exp^{-KC_e})$	q_m (mg g^{-1})	4.479
		K	0.381
		R-square (COD)	0.946
		R^2	0.928
Hill	$q_e = q_m C_e^n /(K + C_e^n)$	q_m (mg g^{-1})	12.590
		K	6.216
		n	0.564
		R-square (COD)	0.995
		R^2	0.990

Fig. 7 Adsorption kinetics of BG adsorption onto poly(DVB).

experimental data and model fittings are illustrated in Fig. 7, while the kinetic parameters and correlation coefficients (R^2) are presented in Table 3. The pseudo-second-order (PSORE)

model assumes that the adsorption process is governed by a chemisorption mechanism, involving electron transfer between the adsorbent and the adsorbate. In contrast, the pseudo-first-order (PFORE) model suggests that the adsorption rate is proportional to the number of unoccupied sites on the adsorbent. The correlation coefficients (R^2) in Table 3 indicate that the PSORE model ($R^2 = 0.838$) provides a better fit to the experimental data than the PFORE model ($R^2 = 0.733$), suggesting that chemisorption is the dominant mechanism controlling the adsorption of BG dye onto poly(DVB). Furthermore, the calculated equilibrium adsorption capacity ($q_e = 4.941$) from the PSORE model is closer to the experimental values than the PFORE model, reinforcing its suitability. The intra-particle diffusion (IPDE) model was applied to evaluate the rate-limiting step of the adsorption process. This model assumes that adsorption can be governed by multiple diffusion processes, including film diffusion, bulk diffusion, and intra-particle diffusion. As shown in Fig. 7, the adsorption capacity (q_t) exhibits a linear relationship with time in the IPDE model, indicating that intra-particle diffusion plays a significant role in the adsorption process. However, the fact that the plot does not pass through the origin suggests other mechanisms, such as surface adsorption and boundary layer effects, may also be

Table 3 Adsorption kinetics of BG adsorption on poly(DVB)

Model	Equation	Parameters	Value
Pseudo-first order	$q_t = q_e(1 - e^{kt})$	q_e (mg g^{-1})	4.462
		k (min^{-1})	0.039
		R-square (COD)	0.745
		R^2	0.733
Pseudo-second order	$q_t = (q_e^2 k_2 t)/(1 + q_e k_2 t)$	q_e (mg g^{-1})	4.941
		k_2 (g mg^{-1} min)	0.013
		R-square (COD)	0.845
		R^2	0.838
Elovich	$q_t = 1/\beta \ln(\alpha\beta t + 1)$	β (g mg^{-1})	0.909
		α (mg g^{-1} min)	0.553
		R-square (COD)	0.942
		R^2	0.942
Intra-particle diffusion	$q_t = k_{diff} t^{0.5} + C$	K_{diff} (mg g^{-1} min$^{-1/2}$)	0.303
		C	1.244
		R-square (COD)	0.901
		R^2	0.897

involved.[59] The Elovich model was employed to describe the chemisorption kinetics of BG onto poly(DVB). This model is typically used for systems where the adsorption rate decreases over time due to surface coverage. The high correlation coefficient ($R^2 = 0.942$) obtained for the Elovich model further supports that the adsorption of BG onto poly(DVB) follows a chemisorption mechanism. Overall, the results indicate that the adsorption of BG onto poly(DVB) is best described by the pseudo-second-order model, suggesting that chemisorption is the primary mechanism. Additionally, intra-particle diffusion significantly contributes to the adsorption process, but it is not the sole rate-limiting step, as indicated by the deviation from linearity in the IPDE model.

3.5. Adsorption thermodynamics

The thermodynamic parameters of BG dye adsorption onto poly(DVB) were evaluated using entropy change (ΔS), enthalpy change (ΔH), and Gibbs free energy change (ΔG) to determine the feasibility and nature of the adsorption process. The relationship between $\ln K_c$ and $1/T$ is depicted in Fig. 8, while the

calculated thermodynamic parameters are summarized in Table 4. To quantify the thermodynamic behavior of adsorption, equilibrium constant (K) was determined using the ratio of the amount of BG dye adsorbed on the poly(DVB) surface at equilibrium (C_{AC}) to the concentration of BG dye remaining in the solution (C_e), as expressed by eqn (6):

$$K = \frac{C_{AC}}{C_e} \tag{6}$$

The temperature dependence of adsorption was evaluated using the Van't Hoff equation (eqn (7)), which establishes a linear relationship between the equilibrium constant (K) and temperature (T):[60,61]

$$\ln K = \frac{\Delta S}{R} - \frac{\Delta H}{RT} \tag{7}$$

where R is the universal gas constant (8.314 J mol^{-1} K^{-1}), and T is the absolute temperature (K). From this equation, the slope and intercept of the $\ln K$ versus $1/T$ plot were used to determine the values of ΔH and ΔS, respectively. The Gibbs free energy change (ΔG), which determines the spontaneity of the adsorption process, was calculated using eqn (8):

$$\Delta G = \Delta H - T\Delta S \tag{8}$$

As observed in Table 4, the negative values of ΔG at all studied temperatures indicate that the adsorption process is
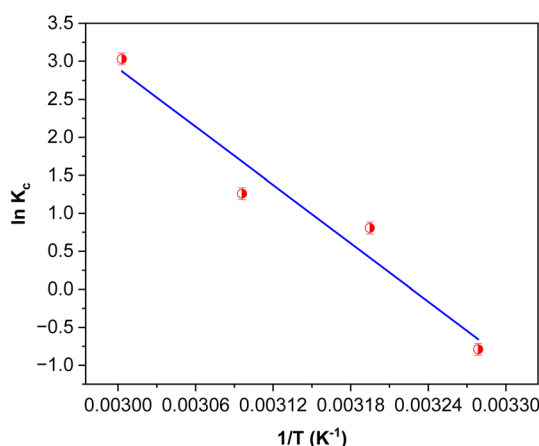

Fig. 8 Plot of $\ln K_c$ against $1/T$ for BG dye adsorption onto poly(DVB).

Table 4 Thermodynamic parameters of BG onto poly(AN-co-AMP)

Temperature (K)	Parameters		
	ΔG (kJ mol^{-1})	ΔH (kJ mol^{-1})	ΔS (J mol^{-1} K^{-1})
305	−104.603	106.3763	343.31
313	−107.35		
323	−110.783		
333	−113.529		

© 2025 The Author(s). Published by the Royal Society of Chemistry

spontaneous. Additionally, the magnitude of ΔG decreases with increasing temperature, suggesting that the adsorption of BG dye onto poly(DVB) becomes more thermodynamically favorable at higher temperatures. This aligns with the increase in adsorption capacity observed experimentally, further confirming the endothermic nature of the process. The positive value of enthalpy change ($\Delta H = 106.3763$ kJ mol^{-1}) confirms that the adsorption of BG dye onto poly(DVB) is endothermic, meaning that higher temperatures enhance the adsorption process. This could be attributed to increased molecular movement at elevated temperatures, which enhances the interaction between the dye molecules and the adsorbent surface.[62] Furthermore, the positive entropy change ($\Delta S = 343.31$ J mol^{-1} K^{-1}) suggests an increase in randomness at the solid–solution interface during adsorption. This indicates that the adsorption process is accompanied by structural changes in the adsorbent–adsorbate system, possibly due to the displacement of pre-adsorbed water molecules and the reorganization of BG dye molecules on the poly(DVB) surface.

3.6. Regeneration study

The recycle experiment is crucial for evaluating the reusability and cost-effectiveness of an adsorbent in practical applications. A highly regenerable adsorbent reduces operational costs and minimizes waste generation, making the process more sustainable. The recycling study was conducted using an adsorption/desorption experiment, where 0.5 M HCl was employed as the desorbing agent to remove the bound BG dye from the poly(DVB) adsorbent.[46] Fig. 9 illustrates the regeneration efficiency of poly(DVB) for BG dye adsorption over four consecutive cycles. The initial removal efficiency was close to 97.4% in the first cycle, with a slight decrease in the second cycle (95.8%). By the third and fourth cycles, the efficiency declined more significantly, reaching approximately 87.8% and 68.7%, respectively. This trend indicates a gradual reduction in the adsorbent's effectiveness after repeated regeneration. The decline in removal efficiency after multiple cycles suggests that

while poly(DVB) retains a considerable adsorption capacity, certain factors contribute to performance loss over successive regenerations. Possible reasons include incomplete desorption of BG molecules, leading to the gradual saturation of active sites, as well as structural or chemical alterations in the polymer matrix due to repeated exposure to acidic conditions. Additionally, partial pore blockage may limit dye accessibility to adsorption sites.[63–65] Despite the decrease in efficiency, the adsorbent maintained a relatively high removal capacity (87.8%) even after three cycles, demonstrating its suitability for multiple uses. However, the more substantial drop observed in the fourth cycle suggests that further optimization of the regeneration process, such as adjusting desorption conditions or employing alternative desorbing agents, may be necessary to enhance long-term reusability. Although poly(DVB) demonstrates superior adsorption capacity and regeneration efficiency, its aromatic, crosslinked structure renders it non-biodegradable under standard environmental conditions. Nevertheless, its environmental impact is mitigated by its reusability, structural stability, and non-leaching nature, making it suitable for safe deployment in water treatment applications. Additionally, poly(DVB) does not degrade into toxic intermediates, and can be safely disposed of through controlled incineration or incorporated into composite waste materials. Future research may focus on developing biodegradable DVB-based composites or greener synthesis strategies to further enhance environmental sustainability.

3.7. Comparison of poly(DVB) with other reported adsorbents

The efficiency of poly(DVB) for the removal of BG dye was compared with various reported adsorbents under different reaction conditions as illustrated in Table 5. The results indicate that poly(DVB) exhibits a high removal efficiency of 97.4%, making it one of the most effective adsorbents for BG dye removal. Among the compared materials, activated carbon (CNSAC) achieved the highest removal efficiency of 99% at a BG dye concentration of 50 mg L^{-1} with a dosage of 0.1 g and a contact time of 90 minutes.[66] While CNSAC demonstrates slightly better performance than poly(DVB), its reaction conditions involve a higher dosage, which raise the cost effect of adsorption process. Other adsorbents, such as ZnO/PPy nanocomposite and polyaniline/silver nanocomposite, exhibited notable removal efficiencies of 90.2%[67] and 90%,[68] respectively. However, these materials required different operating conditions, such as longer contact times or higher initial dye concentrations. Similarly, kaolin, a natural clay-based adsorbent, showed a removal efficiency of 91%,[69] but it required a much higher adsorbent dose of 1 g, making poly(DVB) more efficient in terms of adsorbent usage. Compared to hydroxyapatite/chitosan composite and magnetic RHA, which had removal efficiencies of 80%[24] and 79.4%,[1] respectively, poly(DVB) clearly demonstrates superior adsorption performance. Additionally, these alternative adsorbents required significantly higher dosages (0.5–0.9 g) to achieve their reported efficiencies, whereas poly(DVB) achieved a 97.4% removal rate
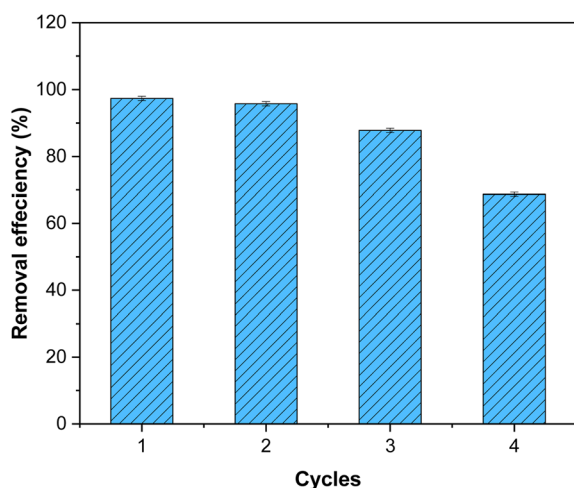
Fig. 9 Regeneration efficiency of poly(DVB) for the adsorption of BG.

Table 5 Comparison of removal efficiency of poly(DVB) with different adsorbents for removal of BG dye

No.	Adsorbent	Reaction condition			Removal (%)	Ref.
		Dye conc. (mg l^{-1})	Dose (g)	Time (min)		
1	Poly (DVB)	7.5	0.05	120	97.4	Present study
2	Hydroxyapatite/chitosan	5	0.9	90	80	24
3	Magnetic RHA	5	0.5	60	79.4	1
4	ZnO/PPy nanocomposite	90	0.075	90	90.2	67
5	Polyaniline/silver nanocomposite	45.45	0.03	120	90	68
6	Kaolin	20	1	90	91	69
7	Ni–Gd(OH)$_3$	10	0.01	300	92	70
8	(CNTS) thin films	10	—	60	91.12	71
9	Activated carbon (CNSAC)	50	0.1	90	99	66
10	Poly(AN-co-AMPS)	7.5	0.1	80	99.5	46

with just 0.1 g of adsorbent. Poly(DVB) emerges as a highly efficient adsorbent for BG dye removal due to its high adsorption capacity, lower required dosage, and competitive removal efficiency compared to other adsorbents. Its reusability potential further enhances its applicability, making it a promising material for dye removal applications in wastewater treatment.

3.8. Atomistic insights into the adsorption mechanism

Our DFT calculations have fully characterized the most stable and favorable binding orientation of the BG dye on the polymer surface. Notably, the BG dye adopts a parallel orientation relative to the polymer surface, which maximizes the π–π interactions between the aromatic moieties of the dye and the polymer (Fig. 10). This alignment, driven by the abundance of π orbitals, facilitates a stable accommodation of the dye on the polymer, potentially explaining the favorable interaction between the two components.

Analysis of the HOMO and LUMO molecular orbitals reveals that the HOMO is primarily localized on the aromatic regions of the polymer, with no contribution from the cationic BG dye. Conversely, the LUMO is distributed over the geometry of the dye, with no involvement from the polymer (Fig. 10). This electronic distribution clearly indicates a chemisorption interaction, where the polymer acts as the electron donor and the cationic dye serves as the electron acceptor. Furthermore, the calculated adsorption energy is −19.14 kJ mol^{-1}, supporting a favorable interaction, consistent with the experimental observations.
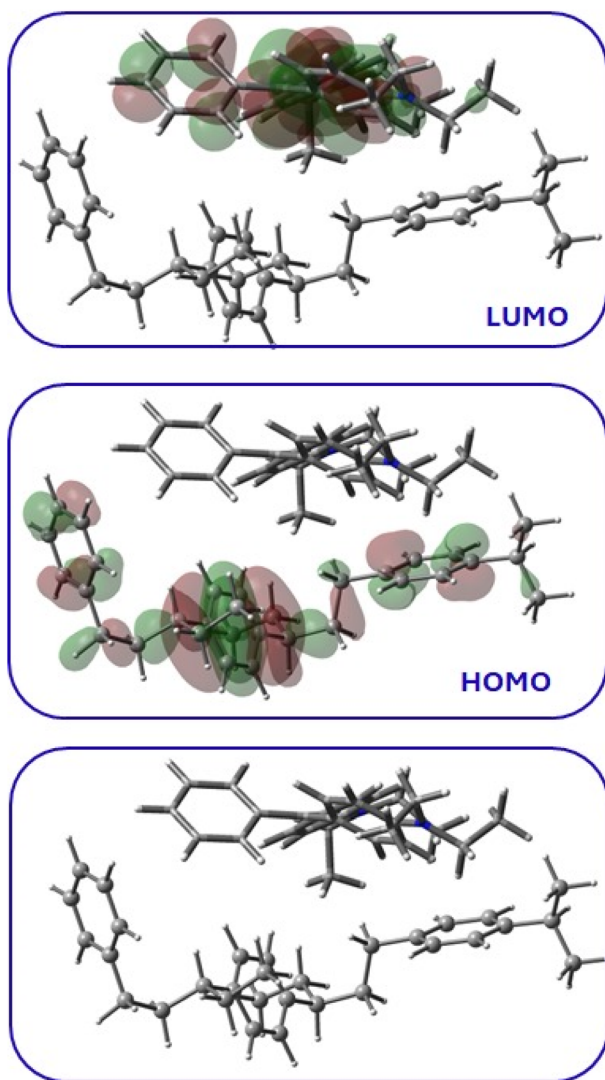

Fig. 10 The optimized molecular geometry for the BG dye (Tube) adsorbed on the surface of the polymer (Ball and stick) together with its HOMO and LUMO.
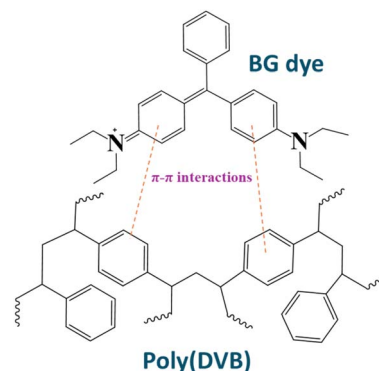

Fig. 11 Schematic representation of the interaction mechanisms between poly(DVB) and BG dye.

Based on the data obtained from DFT calculations and the structure of both BG dye and poly(DVB), we can conclude that the adsorption of BG dye onto poly(DVB) is predominantly governed by $\pi-\pi$ interactions as shown in Fig. 11. BG dye contains multiple aromatic rings in its molecular structure, which can interact with the phenyl groups present in the poly(DVB) matrix through $\pi-\pi$ interaction. The extended conjugated system in BG enhances these interactions, making $\pi-\pi$ stacking a dominant mechanism in the adsorption process.[46] Also, this interaction is further supported by the high surface area and aromatic density of poly(DVB), which provides numerous sites for such interactions and enhancing the adsorption efficiency.

4. Conclusion

This study successfully demonstrated the high adsorption efficiency of poly(DVB) for the removal of brilliant green dye from aqueous solutions. Through extensive physicochemical characterization, poly(DVB) was confirmed to possess a well-developed porous structure, thermal stability, and a high surface area, which contribute to its excellent adsorption performance. Kinetic modeling revealed that the adsorption process followed a pseudo-second-order mechanism, indicating a chemisorption–driven interaction. Isotherm studies showed that the Langmuir model best described the adsorption behavior, confirming monolayer adsorption on a homogeneous surface. Thermodynamic analysis further supported the endothermic and spontaneous nature of the adsorption process, with increased temperature enhancing dye uptake. Additionally, poly(DVB) exhibited notable regeneration efficiency, retaining a high removal capacity after multiple cycles, reinforcing its economic and practical applicability. A comparative analysis with other reported adsorbents demonstrated that poly(DVB) offers competitive advantages, including high removal efficiency at lower adsorbent dosages and favorable reusability. Using DFT calculation we provided interpretation on the obtained favorable chemical interaction of the adsorption process. The obtained chemisorption process has resulted from aromatic–aromatic interactions where the BG dye will mainly act as an electron acceptor while the polymer behaves as electron donor. These findings suggest that poly(DVB) is a promising candidate for large-scale wastewater treatment applications, offering an efficient, and sustainable solution for mitigating dye pollution in aquatic environments. Another point we must take in our consideration, While poly(DVB) demonstrated excellent adsorption performance and reusability, its non-biodegradability, potential challenges in large-scale production, and the need for long-term stability assessments under real wastewater conditions remain limitations that should be addressed in future studies.

Data availability

The data that support the findings of this study are available from the corresponding author upon reasonable request.

Author contributions

Marwa Magd: experiments, analysis, project administration, resources, writing – review & editing; Mohamed Aboelnga, project administration, calculation, investigation, writing – review & editing; Aya Dyab: investigation, data curation, Aliaa Semida, methodology, data curation, Nada Elseady, methodology, investigation, Mona Abo Hashesh, calculation, visualization, Rawan Rizk, methodology, writing – original draft; Elsayed Elbayoumy: project administration, conceptualization, validation, formal analysis, investigation, resources, data curation, writing – review & editing.

Conflicts of interest

The authors declare that they have no known competing financial interests or personal relationships that could have appeared to influence the work reported in this paper.

References

1 I. Dahlan, H. M. Zwain, M. A. O. Seman, N. H. Baharuddin and M. R. Othman, Adsorption of brilliant green dye in aqueous medium using magnetic adsorbents prepared from rice husk ash, *AIP Conf. Proc.*, 2019, **2124**, 020017.

2 E. Elbayoumy, M. O. Elassi, G. M. Khairy, E. A. Moawed and M. M. aboelnga, Development of efficient fluorescent sensor for the detection of hazard aromatic nitro compounds *via* N-(1-naphthyl)ethylenediamine: Experimental and DFT studies, *J. Mol. Liq.*, 2023, **391**, 123270.

3 E. Elbayoumy, M. Shaker, M. Gaafar, E. A. Moawed and M. M. Aboelnga, Eco-friendly one-step production of a highly sensitive fluorescent sensor for iron (III) detection in aqueous solutions: Experimental and DFT insights, *J. Photochem. Photobiol., A*, 2025, **466**, 116391.

4 P. Parthipan, L. Cheng, A. Rajasekar, M. Govarthanan and A. Subramania, Biologically reduced graphene oxide as a green and easily available photocatalyst for degradation of organic dyes, *Environ. Res.*, 2021, **196**, 110983.

5 M. Berradi, R. Hsissou, M. Khudhair, M. Assouag, O. Cherkaoui, A. El Bachiri, *et al.*, Textile finishing dyes and their impact on aquatic environs, *Heliyon*, 2019, **5**, e02711.

6 H. B. Slama, A. C. Bouket, Z. Pourhassan, F. N. Alenezi, A. Silini, H. Cherif-Silini, *et al.*, Diversity of synthetic dyes from textile industries, discharge impacts and treatment methods, *Appl. Sci.*, 2021, **11**(14), 6255.

7 A. Singh, D. B. Pal, A. Mohammad, A. Alhazmi, S. Haque, T. Yoon, *et al.*, Biological remediation technologies for dyes and heavy metals in wastewater treatment: New insight, *Bioresour. Technol.*, 2022, **343**, 126154.

8 S. Agarwal, V. K. Gupta, M. Ghasemi and J. Azimi-Amin, Peganum harmala-L Seeds adsorbent for the rapid removal of noxious brilliant green dyes from aqueous phase, *J. Mol. Liq.*, 2017, **231**, 296–305.

9 K. Sukla Baidya and U. Kumar, Adsorption of brilliant green dye from aqueous solution onto chemically modified areca nut husk, *S. Afr. J. Chem. Eng.*, 2021, **35**, 33–43.

10 V. K. Gupta, A. Nayak and S. Agarwal, Bioadsorbents for remediation of heavy metals: Current status and their future prospects, *Environ. Eng. Res.*, 2015, **20**(1), 1–18.

11 S. Chowdhury, R. Mishra, P. Saha and P. Kushwaha, Adsorption thermodynamics, kinetics and isosteric heat of adsorption of malachite green onto chemically modified rice husk, *Desalination*, 2011, **265**(1–3), 159–168.

12 A. M. Aljeboree, N. D. Radia, L. S. Jasim, A. A. Alwarthan, M. M. Khadhim, A. Washeel Salman, *et al.*, Synthesis of a new nanocomposite with the core TiO2/hydrogel: Brilliant green dye adsorption, isotherms, kinetics, and DFT studies, *J. Ind. Eng. Chem.*, 2022, **109**, 475–485.

13 V. K. Gupta, T. I. Suhas, S. Agarwal, R. Singh, M. Chaudhary, *et al.*, Column operation studies for the removal of dyes and phenols using a low cost adsorbent, *Global J. Environ. Sci. Manage.*, 2016, **2**(1), 1–10.

14 A. Mittal, V. Gajbe and J. Mittal, Removal and recovery of hazardous triphenylmethane dye, Methyl Violet through adsorption over granulated waste materials, *J. Hazard. Mater.*, 2008, **150**(2), 364–375.

15 N. Laskar and U. S. E. M. Kumar, FTIR and EDAX Studies for the Removal of Safranin Dye from Water Bodies using Modified Biomaterial - Bambusa Tulda, *IOP Conf. Ser.:Mater. Sci. Eng.*, 2017, **225**, 012105.

16 M. Ghaedi, G. Negintaji, H. karimi and F. Marahel, Solid phase extraction and removal of brilliant green dye on zinc oxide nanoparticles loaded on activated carbon: New kinetic model and thermodynamic evaluation, *J. Ind. Eng. Chem.*, 2014, **20**(4), 1444–1452.

17 M. Oplatowska, R. F. Donnelly, R. J. Majithiya, D. Glenn Kennedy and C. T. Elliott, The potential for human exposure, direct and indirect, to the suspected carcinogenic triphenylmethane dye Brilliant Green from green paper towels, *Food Chem. Toxicol.*, 2011, **49**(8), 1870–1876.

18 A. F. Ali, A. S. Kovo and S. A. Adetunji, Methylene Blue and Brilliant Green Dyes Removal from Aqueous Solution Using Agricultural Wastes Activated Carbon, *J. Encapsulation Adsorpt. Sci.*, 2017, **7**(2), 95–107.

19 X. Yan, M. Chen, J. Wang, Z. Wang, R. Xin, D. Wu, *et al.*, Nanoarchitectonics of bamboo-based heterojunction photocatalyst for effective removal of organic pollutants, *Chem. Eng. J.*, 2024, **495**, 153431. Available from: https://www.sciencedirect.com/science/article/pii/S1385894724049209.

20 A. B. Bassa, O. A. Zelekew, T. A. Meresa and T. A. Berhe, Croton macrostachyus leaf-mediated biosynthesis of copper oxide nanoparticles for enhanced catalytic reduction of organic dyes, *Mater. Res. Express*, 2024, **11**(8), 085001.

21 B. K. Nandi and S. Patel, Effects of operational parameters on the removal of brilliant green dye from aqueous solutions by electrocoagulation, *Arabian J. Chem.*, 2017, **10**, S2961–S2968, DOI: 10.1016/j.arabjc.2013.11.032.

22 M. A. Dominguez, M. Etcheverry and G. P. Zanini, Evaluation of the adsorption kinetics of brilliant green dye onto a montmorillonite/alginate composite beads by the shrinking core model, *Adsorption*, 2019, **25**(7), 1387–1396, DOI: 10.1007/s10450-019-00101-w.

23 D. Robati, B. Mirza, M. Rajabi, O. Moradi, I. Tyagi, S. Agarwal, *et al.*, Removal of hazardous dyes-BR 12 and methyl orange using graphene oxide as an adsorbent from aqueous phase, *Chem. Eng. J.*, 2016, **284**, 687–697, DOI: 10.1016/j.cej.2015.08.131.

24 A. Ragab, I. Ahmed and D. Bader, The removal of Brilliant Green dye from aqueous solution using nano hydroxyapatite/chitosan composite as a sorbent, *Molecules*, 2019, **24**(5), 847.

25 S. Singh, H. Gupta, S. Dhiman and N. Kishore, Decontamination of cationic dye brilliant green from the aqueous media, *Appl. Water Sci.*, 2022, **12**(4), 1–10, DOI: 10.1007/s13201-022-01596-5.

26 M. Luna Quinto, S. Khan, J. Vega-Chacón, B. Mortari, A. Wong, M. D. P. Taboada Sotomayor, *et al.*, Development and Characterization of a Molecularly Imprinted Polymer for the Selective Removal of Brilliant Green Textile Dye from River and Textile Industry Effluents, *Polymers*, 2023, **15**(18), 3709.

27 M. R. El-Aassar, O. M. Ibrahim, B. M. Omar, H. T. A. El-Hamid, I. H. Alsohaim, H. M. A. Hassan, *et al.*, Hybrid Beads of Poly(Acrylonitrile-co-Styrene/Pyrrole)@Poly Vinyl Pyrrolidone for Removing Carcinogenic Methylene Blue Dye Water Pollutant, *J. Polym. Environ.*, 2023, **31**(7), 2912–2929, DOI: 10.1007/s10924-023-02776-3.

28 M. M. Altayan, N. Tzoupanos and M. Barjenbruch, Polymer based on beta-cyclodextrin for the removal of bisphenol A, methylene blue and lead(II): Preparation, characterization, and investigation of adsorption capacity, *J. Mol. Liq.*, 2023, **390**, 122822. Available from: https://www.sciencedirect.com/science/article/pii/S0167732223016276.

29 E. Elbayoumy, Y. Wang, J. Rahman, C. Trombini, M. Bando, Z. Song, *et al.*, Pd Nanoparticles-Loaded Vinyl Polymer Gels: Preparation, Structure and Catalysis, *Catalysts*, 2021, **11**(1), 137.

30 F. M. B. Coutinho, M. A. F. S. Neves and M. L. Dias, Porous Structure and Swelling Properties of Styrene–Divinylbenzene Copolymers for Size Exclusion Chromatography, *J. Appl. Polym. Sci.*, 1997, **65**(7), 1257–1262.

31 M. Frisch, G. Trucks, H. Schlegel, G. Scuseria, M. Robb and J. Cheeseman, *et al.*, *Gaussian 16, Revision a. 03, wallingford ct. Gaussian16 (Revision A 03)*, Gaussian, inc., 2016.

32 P. J. Stephens, F. J. Devlin, C. F. Chabalowski and M. J. Frisch, Ab Initio Calculation of Vibrational Absorption and Circular Dichroism Spectra Using Density Functional Force Fields, *J. Phys. Chem.*, 1994, **98**(45), 11623–11627.

33 A. D. Becke, Density-functional thermochemistry. III. The role of exact exchange, *J. Chem. Phys.*, 1993, **98**(7), 5648–5652.

34 J. P. Perdew, M. Ernzerhof and K. Burke, Rationale for mixing exact exchange with density functional approximations, *J. Chem. Phys.*, 1996, **105**(22), 9982–9985.

35 M. M. Aboelnga, J. J. Hayward and J. W. Gauld, Enzymatic Post-Transfer Editing Mechanism of *E. coli* Threonyl-tRNA Synthetase (ThrRS): A Molecular Dynamics (MD) and Quantum Mechanics/Molecular Mechanics (QM/MM) Investigation, *ACS Catal.*, 2017, **7**(8), 5180–5193.

36 M. M. Aboelnga, J. J. Hayward and J. W. Gauld, Unraveling the Critical Role Played by $_{Ado76}2'OH$ in the Post-Transfer Editing by Archaeal Threonyl-tRNA Synthetase, *J. Phys. Chem. B*, 2018, **122**(3), 1092–1101.

37 M. S. Mohy Eldin, Y. A. Aggour, M. R. El-Aassar, G. E. Beghet and R. R. Atta, Development of nano-crosslinked polyacrylonitrile ions exchanger particles for dyes removal, *Desalin. Water Treat.*, 2016, **57**(9), 4255–4266.

38 E. Elbayoumy, A. A. El-Bindary, T. Nakano and M. M. Aboelnga, Silver nanoparticles immobilized on crosslinked vinyl polymer for catalytic reduction of nitrophenol: experimental and computational studies, *Sci. Rep.*, 2025, **15**(1), 717.

39 M. Fathy, T. Abdel Moghny, A. E. Awad Allah and A. E. Alblehy, Cation exchange resin nanocomposites based on multi-walled carbon nanotubes, *Appl. Nanosci.*, 2014, **4**(1), 103–112.

40 E. Elbayoumy, N. A. El-Ghamaz, F. S. Mohamed, M. A. Diab and T. Nakano, Dielectric permittivity, AC electrical conductivity and conduction mechanism of high crosslinked-vinyl polymers and their Pd(OAc)2 composites, *Polymers*, 2021, **13**(17), 3005.

41 Y. A. Aggour, E. R. Kenawy, M. Magdy and E. Elbayoumy, Establishing a productive heterogeneous catalyst based on silver nanoparticles supported on a crosslinked vinyl polymer for the reduction of nitrophenol, *RSC Adv.*, 2024, **14**(41), 30127–30139.

42 E. Elbayoumy, M. Elhendawy, M. M. Gaafar, E. A. Moawed and M. M. aboelnga, Novel fluorescent sensor based on triazole-pyridine derivative for selective detection of mercury (II) ions in different real water samples: Experimental and DFT calculations, *J. Mol. Liq.*, 2024, **401**, 124589. Available from: **https://www.sciencedirect.com/science/article/pii/S0167732224006457**.

43 N. A. El-ghamaz, T. S. Ahmed and D. A. Salama, Optical , dielectrical properties and conduction mechanism of copolymer (N , N ′ -bissulphinyl- m -benzenediamine- p -phenylenediamine), *Eur. Polym. J.*, 2017, **93**, 8–20, DOI: **10.1016/j.eurpolymj.2017.05.022**.

44 S. K. Akay, A. Peksoz and A. Kara, Magnetic responses of divinylbenzene-Fe3O4 composite film deposited by free radical polymerization method, *J. Supercond. Novel Magn.*, 2018, **31**(3), 849–854.

45 B. D. Zdravkov, J. J. Čermák, M. Šefara and J. Janků, Pore classification in the characterization of porous materials: A perspective, *Cent. Eur. J. Chem.*, 2007, **5**(2), 385–395.

46 Y. A. Aggour, E. R. Kenawy, M. Magdy and E. Elbayoumy, Multifunctional copolymers for brilliant green dye removal: adsorption kinetics, isotherm and process optimization, *Environ. Sci.:Adv.*, 2025, **4**, 787–808.

47 K. Sukla and U. Kumar, South African Journal of Chemical Engineering Adsorption of brilliant green dye from aqueous solution onto chemically modified areca nut husk, *S. Afr. J. Chem. Eng.*, 2021, **35**, 33–43, DOI: **10.1016/j.sajce.2020.11.001**.

48 A. Soltani, M. Faramarzi and S. A. M. Parsa, A review on adsorbent parameters for removal of dye products from industrial wastewater, *Water Qual. Res. J.*, 2021, **56**, 181–193.

49 M. Ali Khan, R. Govindasamy, A. Ahmad, M. R. Siddiqui, S. A. Alshareef, A. A. Hakami, *et al.*, Carbon Based Polymeric Nanocomposites for Dye Adsorption: Synthesis, Characterization, and Application, *Polymers*, 2021, **13**.

50 K. Y. Foo and B. H. Hameed, Insights into the modeling of adsorption isotherm systems, *Chem. Eng. J.*, 2010, **156**(1), 2–10.

51 G. Y. Abate, A. N. Alene, A. T. Habte and D. M. Getahun, Adsorptive removal of malachite green dye from aqueous solution onto activated carbon of Catha edulis stem as a low cost bio-adsorbent, *Environ. Syst. Res.*, 2020, **9**, 29, DOI: **10.1186/s40068-020-00191-4**.

52 M. T. Yagub, T. K. Sen, S. Afroze and H. M. Ang, Dye and its removal from aqueous solution by adsorption: A review, *Adv. Colloid Interface Sci.*, 2014, **209**, 172–184. Available from: **https://www.sciencedirect.com/science/article/pii/S0001868614001389**.

53 J. Hou, Y. Zhou, J. Shan, C. Gu, T. Zhang and B. Wu, Quinoline and cholesterol based organogelator for selective adsorption of cationic dyes, *Colloids Surf., A*, 2024, **700**, 134851, DOI: **10.1016/j.colsurfa.2024.134851**.

54 A. Fathi, E. Asgari, H. Danafar, H. salehabadi and M. M. Fazli, A comprehensive study on methylene blue removal via polymer and protein nanoparticle adsorbents, *Sci. Rep.*, 2024, **14**(1), 29434.

55 T. M. Budnyak, M. Błachnio, A. Slabon, A. Jaworski, V. A. Tertykh, A. Deryło-Marczewska, *et al.*, Chitosan Deposited onto Fumed Silica Surface as Sustainable Hybrid Biosorbent for Acid Orange 8 Dye Capture: Effect of Temperature in Adsorption Equilibrium and Kinetics, *J. Phys. Chem. C*, 2020, **124**(28), 15312–15323, DOI: **10.1021/acs.jpcc.0c04205**.

56 R. G. El-Sharkawy, Anchoring of green synthesized silver nanoparticles onto various surfaces for enhanced heterogeneous removal of brilliant green dye from aqueous solutions with error analysis study, *Colloids Surf., A*, 2019, **583**, 123871, DOI: **10.1016/j.colsurfa.2019.123871**.

57 T. A. Saleh, Chapter 4 – Isotherm models of adsorption processes on adsorbents and nanoadsorbents, in *Surface Science of Adsorbents and Nanoadsorbents*, ed. T. Saleh, Elsevier, 2022. pp. 99–126.

58 A. I. Adeogun, M. A. Idowu, A. E. Ofudje, S. O. Kareem and S. A. Ahmed, Comparative biosorption of Mn(II) and Pb(II) ions on raw and oxalic acid modified maize husk: Kinetic,

thermodynamic and isothermal studies, *Appl. Water Sci.*, 2013, **3**(1), 167–179.

59 S. P. Dharmarathna and N. Priyantha, Investigation of boundary layer effect of intra-particle diffusion on methylene blue adsorption on activated carbon, *Energy Nexus*, 2024, **14**, 100294.

60 X. Zhou, X. Yu, R. Maimaitiniyazi, X. Zhang and Q. Qu, Discussion on the thermodynamic calculation and adsorption spontaneity re Ofudje *et al.* (2023), *Heliyon*, 2024, **10**(8), e28188.

61 E. C. Lima, A. A. Gomes and H. N. Tran, Comparison of the nonlinear and linear forms of the van't Hoff equation for calculation of adsorption thermodynamic parameters ($\Delta S°$ and $\Delta H°$), *J. Mol. Liq.*, 2020, **311**, 113315.

62 C. A. Guerrero-Fajardo, L. Giraldo and J. C. Moreno-Pirajan, Isotherm, thermodynamic, and kinetic studies of dye adsorption on graphene oxides with varying oxidation degrees, *Results Eng.*, 2025, **26**, 104558.

63 Y. Tamer and H. Berber, Kinetic, isotherm, and thermodynamic studies for adsorptive removal of basic violet 14 from aqueous solution, *Turk. J. Chem.*, 2022, **46**(6), 2057–2071.

64 S. Sudarsan, G. Murugesan, T. Varadavenkatesan, R. Vinayagam and R. Selvaraj, Efficient adsorptive removal of Congo Red dye using activated carbon derived from Spathodea campanulata flowers, *Sci. Rep.*, 2025, **15**(1), 1831.

65 F. Liu, Z. Guo, H. Ling, Z. Huang and D. Tang, Effect of pore structure on the adsorption of aqueous dyes to ordered mesoporous carbons, *Microporous Mesoporous Mater.*, 2016, **227**, 104–111.

66 P. Samiyammal, A. Kokila, L. A. Pragasan, R. Rajagopal, R. Sathya, S. Ragupathy, *et al.*, Adsorption of brilliant green dye onto activated carbon prepared from cashew nut shell by KOH activation: Studies on equilibrium isotherm, *Environ. Res.*, 2022, **212**, 113497, DOI: **10.1016/j.envres.2022.113497**.

67 M. Zhang, L. Chang, Y. Zhao and Z. Yu, Fabrication of Zinc Oxide/Polypyrrole Nanocomposites for Brilliant Green Removal from Aqueous Phase, *Arabian J. Sci. Eng.*, 2019, **44**(1), 111–121.

68 O. Abd Al-Qader Mahmood and B. I. Waisi, Synthesis and characterization of polyacrylonitrile based precursor beads for the removal of the dye malachite green from its aqueous solutions, *Desalin. Water Treat.*, 2021, **216**, 445–455.

69 B. K. Nandi, A. Goswami and M. K. Purkait, Adsorption characteristics of brilliant green dye on kaolin, *J. Hazard. Mater.*, 2009, **161**(1), 387–395.

70 S. N. Matussin, F. Khan, M. H. Harunsani, Y. M. Kim and M. M. Khan, Photocatalytic degradation of brilliant green and 4-nitrophenol using Ni-doped Gd(OH)3 nanorods, *Sci. Rep.*, 2024, **14**(1), 8269.

71 A. Nezzari, S. Medina, Y. Khane, H. Boublenza, M. Guezzoul, A. Zoukel, *et al.*, Synthesis, properties, and photocatalytic degradation of Brilliant Green dye using Cu2NiSnS4 thin films under ultraviolet irradiation, *Inorg. Chem. Commun.*, 2025, **174**, 114021.